Icarus 205 (2010) 230–243

Contents lists available at ScienceDirect

Icarus

journal homepage: www.elsevier.com/locate/icarus

Emplacement of the youngest flood lava on Mars: A short, turbulent story

W.L. Jaeger [a,*], L.P. Keszthelyi [a], J.A. Skinner Jr. [a], M.P. Milazzo [a], A.S. McEwen [b], T.N. Titus [a], M.R. Rosiek [a], D.M. Galuszka [a], E. Howington-Kraus [a], R.L. Kirk [a], the HiRISE Team

[a] US Geological Survey, 2255 N. Gemini Dr., Flagstaff, AZ 86001, United States
[b] Lunar and Planetary Laboratory, University of Arizona, Tucson, AZ 85721, United States

ARTICLE INFO

Article history:
Received 14 November 2008
Revised 12 August 2009
Accepted 2 September 2009
Available online 29 September 2009

Keywords:
Geological processes
Mars, Surface
Volcanism

ABSTRACT

Recently acquired data from the High Resolution Imaging Science Experiment (HiRISE), Context (CTX) imager, and Compact Reconnaissance Imaging Spectrometer for Mars (CRISM) onboard the *Mars Reconnaissance Orbiter* (*MRO*) spacecraft were used to investigate the emplacement of the youngest flood-lava flow on Mars. Careful mapping finds that the Athabasca Valles flood lava is the product of a single eruption, and it covers 250,000 km^2 of western Elysium Planitia with an estimated 5000–7500 km^3 of mafic or ultramafic lava. Calculations utilizing topographic data enhanced with *MRO* observations to refine the dimensions of the channel system show that this flood lava was emplaced turbulently over a period of only a few to several weeks. This is the first well-documented example of a turbulently emplaced flood lava anywhere in the Solar System. However, *MRO* data suggest that this same process may have operated in a number of martian channel systems. The magnitude and dynamics of these lava floods are similar to the aqueous floods that are generally believed to have eroded the channels, raising the intriguing possibility that mechanical erosion by lava could have played a role in their incision.

1. Introduction

Flood lavas are very fluid lava flows that travel long distances and spread out to cover broad areas (e.g., Richthofen, 1868; Geikie, 1880; Washington, 1922; Tyrrell, 1937). They do not build tall volcanoes by repeatedly erupting from a central vent. Instead, flood lavas issue from vast fissure systems and inundate the pre-existing landscape, often leveling it by infilling basins and other low-lying terrain.

The notion that flood lavas may be emplaced turbulently has waxed and waned in the scientific literature over the past few decades. The first quantitative study of flood-lava emplacement was conducted by Shaw and Swanson (1970). Looking specifically at the Roza Member of the Wanapum Basalt within the Columbia River Basalt Group (CRBG), they concluded from fluid dynamic calculations that the 30-m-thick flow was emplaced as a turbulent flood over a period of weeks. They estimated the flux of lava to be of order 10^6 m^3/s, which is comparable to the estimated flux of the catastrophic water floods that later carved the Channeled Scabland into the CRBG (e.g., Baker, 1973). This paradigm was widely accepted as the archetypal flood-lava emplacement mechanism for more than two decades (e.g., Hooper, 1982; Huppert and Sparks, 1985; Reidel and Fecht, 1987; Reidel and Tolan, 1992). By extension, the idea of turbulent lava flows was also applied to extraterrestrial lavas. For example, Hulme (1973) suggested that sinuous rilles on the Moon were carved by turbulent lava flows erupted at high rates, and Komatsu et al. (1992) suggested a similar process (though one involving exotic lava compositions) for the formation of canali on Venus.

A paradigm shift away from turbulent emplacement began to take place in the mid 1990s, when the "inflation" process was documented in active Hawaiian lava flows (Hon et al., 1994). By this process, the solidified crust that floats on a molten sheet of lava is gradually lifted, as the molten layer thickens due to the continued influx of fluid lava. Following the Hon et al. (1994) study, researchers identified features diagnostic of inflation in the same CRBG unit that Shaw and Swanson (1970) had previously investigated (Self et al., 1996, 1997; Thordarson and Self, 1998). From the thickness of the inflated (slowly lifted) crust, the eruption duration was determined to be about a decade, corresponding to an average eruption rate in the range of 10^3–10^4 m^3/s (e.g., Self et al., 1997; Thordarson and Self, 1998). Subsequently, inflated sheet flows were found to be common throughout the CRBG and in other flood lava provinces (Self et al., 1998). Therefore, the slow process of inflation was deemed the "standard way of emplacing long lava flows" (i.e. the SWELL hypothesis) (Self et al., 1998).

Although the most detailed work on flood lavas is still that derived from studies of terrestrial flows, an abundance of high-quality spacecraft data has spawned investigations of similar features on other rocky bodies throughout the Solar System. To

* Corresponding author. Address: US Geological Survey, Astrogeology Research Program, 2255 N. Gemini Dr., Flagstaff, AZ 86001, United States.
E-mail address: wjaeger@usgs.gov (W.L. Jaeger).

0019-1035/$ - see front matter © 2009 Published by Elsevier Inc.
doi:10.1016/j.icarus.2009.09.011

date, flood lavas in various stages of preservation have been identified on the Moon, Venus, Mars, the jovian moon Io, and (tentatively) Mercury (e.g., BVSP, 1981; Head and Coffin, 1997; Keszthelyi et al., 2006; Wilson and Head, 2008). Collectively, these extraterrestrial flood lavas show more diversity than is reported for Earth alone. For example, some flood lavas on Io appear to be fed by lava tubes at rates of order 10^2 m^3/s, which is at least an order of magnitude slower than their terrestrial counterparts (e.g., Keszthelyi et al., 2006). In contrast, many martian flood lavas have physical characteristics suggestive of rapidly emplaced sheet flows such as a surface of rafted plates and pressure ridges (Keszthelyi et al., 2000) that appear morphologically similar to pack ice (Murray et al., 2005). Preliminary modeling by Keszthelyi et al. (2000, 2004) estimated the average eruption rate for these "platy-ridged" martian flood lavas to be of order 10^4 m^3/s, with surges to 10^5 m^3/s, thus advancing the idea of rapid laminar emplacement.

While the discovery of platy-ridged lavas on Mars has greatly enhanced our understanding of the process of flood volcanism, the quantitative modeling was limited by the inability to determine: (a) the dimensions of individual lava flows and (b) the details of the flow dynamics. These problems can now be addressed with the suite of instruments onboard the *Mars Reconnaissance Orbiter* (*MRO*) spacecraft. In particular, the High Resolution Imaging Science Experiment (HiRISE) camera and the Context (CTX) imager, allow the martian flood lavas to be investigated in an unprecedented combination of detail and breadth.

2. The Athabasca Valles flood lava

The best preserved, and presumably youngest, flood lavas on Mars occur in the equatorial plains of Elysium Planitia (e.g., Plescia, 1990) (Fig. 1). Impact crater size-frequency distributions indicate a Late Amazonian (<0.6 Ga) age for these volcanic plains (Hartmann and Neukum, 2001; Berman and Hartmann, 2002), which comprise a mix of flood lavas erupted from the Cerberus Fossae fissure system and lava flows fed from a series of low shields collectively known as the Cerberus Tholi. Within the Elysium Planitia volcanic province, the youngest and best-exposed flood lava is that which flowed through Athabasca Valles.

Athabasca Valles is an outflow channel system located in north-central Elysium Planitia. It emerges full-born from the westernmost major fissure segment of the Cerberus Fossae, stretches southwest for ~300 km, and empties into the Cerberus Palus basin (Fig. 1). Previous work has shown that, despite the erosional appearance of its gross morphology, the entire channel system (including its banks) is coated with a veneer of lava (Jaeger et al., 2007). The lava is exceedingly thin in proximal Athabasca Valles and gradually thickens in the downstream direction, transitioning from a material unit that drapes the substrate topography to one that submerges it near the terminus of the channel system. The most straightforward interpretation of these observations is that a fissure eruption at the head of Athabasca Valles flooded the down-slope terrain with lava, and then, as the eruption waned, the lava receded from the channels and drained downstream into Cerberus Palus where it ponded (Jaeger et al., 2007). This model

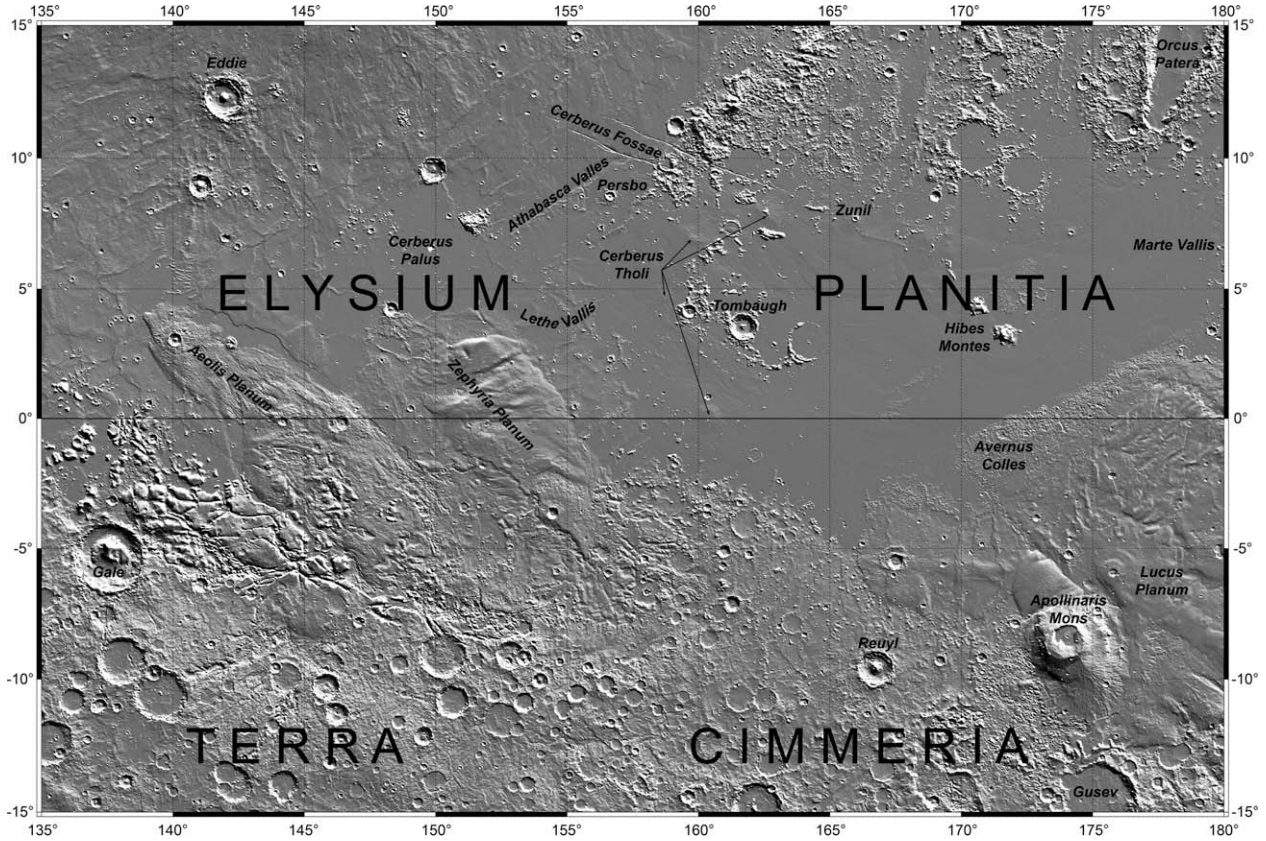

Fig. 1. Location map of selected geographic features in Elysium Planitia. The basemap is a shaded relief image built from the Mars Orbiter Laser Altimeter (MOLA) gridded data. Key features referred to in the text, as well as other major landforms, are labeled. The hemispheric dichotomy boundary, a sharp topographic step that divides the heavily cratered southern highlands from the smoother northern lowlands, fluctuates within 5° of Mars' equator in this region, separating Terra Cimmeria from Elysium Planitia. The smooth plains of Elysium Planitia are covered by lavas that erupted from the Cerberus Fossae (fissures) and the Cerberus Tholi (shields). The youngest major eruption inundated Athabasca Valles (upper middle), the most pristine outflow channel system in the region. Data from the Mars Exploration Rover *Spirit*, which is operating in Gusev crater (lower right), is employed to study this lava flow. Corinto crater lies just beyond the edge of this map, north of Eddie crater (upper left).

is concordant with all of the available data, including the superposition and crosscutting relationships seen in the rootless cones (pseudocraters) that pepper the floor of Athabasca Valles (Jaeger et al., 2007, 2008). Thus, the flood lava that now occupies Athabasca Valles deflated, rather than inflated, in its proximal reaches before solidifying. This emplacement style differs markedly from the SWELL hypothesis.

The emplacement of this flood lava occurred in a geological instant, producing a material unit with a specific lithology at a distinct time horizon (i.e., a lithochronostratigraphic unit). The convention in terrestrial geology is to name such units by their locality and lithology (e.g., Wanapum Basalt). In this case, the obvious locality is "Athabasca Valles". The lithology, however, is more elusive because of limited compositional information (see Section 2.2). All that can be said with certainty is that it is a flood lava. Therefore, we will refer to this unit herein as the Athabasca Valles flood lava, with geologic map symbol abbreviation Aav, where "A" denotes that it is Amazonian in age (see Section 2.1) and "av" refers to Athabasca Valles.

2.1. Absolute and relative age relationships of Aav

The lava that coats the surface of Athabasca Valles is so young that there is a dearth of large impact craters with which to date its surface. The craters that do exist are small (where crater production functions are least certain and target strength can have the greatest effect), and those in the 10–100 m diameter range are dominated by secondaries from the rayed-crater Zunil (McEwen et al., 2005). Berman and Hartmann (2002) derived an age of <20 Ma for Aav, incorporating some of the uncertainties in small crater production rates. More recently, Murray et al. (2005) obtained a model age of 5 ± 2 Ma for the same unit; however, they also suggested that adjacent surfaces on this single flow show a statistically significant age difference of ~1 Ma, raising questions about the adequacy of their reported uncertainties, especially those pertaining to the effect of target strength on the formation of small craters.

More robust, but looser, constraints on the absolute age of Aav can be derived from larger impacts in the region. As noted above, the superposition of Zunil secondaries on Aav makes it incontrovertible that Aav was emplaced prior to the Zunil impact event. Kreslavsky (2008) provided the most complete age estimate for Zunil, including new results on the current cratering rate and the effects of atmospheric breakup, resulting in a model age of ~500 ka. In contrast, Aav has a more cryptic relationship with secondaries from Corinto crater (16.9°N, 141.7°E) (McEwen et al., this issue), which has a Hartmann-function crater age between 10 and 100 Ma (unpublished data from McEwen et al.). In Thermal Emission Imaging System nighttime IR data, wispy rays radial to Corinto extend across the Aav margin in Cerberus Palus. Higher resolution visible images confirm that these rays contain elevated concentrations of small, irregular (presumably secondary) craters. However, the small crater density within individual rays markedly decreases where they cross onto Aav surfaces (cf. Mars Orbiter Camera image M04-04121, CTX image P19_008463_1870_XN_07N212W and HiRISE observations PSP_007448_1845 and ESP_012788_1860). This is likely to be merely a target strength effect wherein the young lava surface is relatively resistant to small impacts, but it is also possible that the small craters observed on Aav are unrelated to Corinto and that their spatial association with the nighttime IR rays is coincidental. Thus, the absolute age of Aav is >0.5 Ma, based on the superposition of Zunil secondaries, and probably >10 Ma, based on the tentative superposition of Corinto secondaries.

While remarkably pristine in morphology, the surface of the Athabasca Valles flood lava has been modified by a variety of geological processes. Many areas have been exhumed by the wind from underneath a mantling deposit. Discontinuous portions of this cover are commonly preserved in the boulder-strewn ejecta blankets of Zunil secondaries (Fig. 2), suggesting that the mantling deposit was aerially extensive but relatively thin (because secondaries penetrate through to the lava substrate) at the time of the Zunil impact event. Other evidence for eolian exhumation can be found at the southern margin of Cerberus Palus, where a particularly young and actively eroding member of the Medusae Fossae Formation (MFF) buries a distal section of Aav (e.g., Lanagan, 2004).

In addition to exhumation, the Athabasca Valles flood lava has been modified by tectonism; it has been locally faulted in extension and, to a lesser extent, compression (Fig. 3), suggesting that it may be older than its surface would otherwise appear. Nonetheless, it is possible that the extensional faulting was triggered by the emptying of a deep magma chamber under the Cerberus Fossae and the resultant subsidence of the overburden, making graben formation a byproduct of the Aav eruption rather than a separate tectonic event. In contrast, the post-emplacement compressional faulting of Aav, which is best seen in northern Cerberus Palus, is due to renewed uplift along wrinkle ridges that predate the Athabasca Valles flood lava. The post-Aav slip on those pre-existing faults appears to be small in magnitude (Fig. 3b).

2.2. Composition of Aav

The chemical makeup of Aav has not been directly measured, but several lines of evidence point to a mafic to ultramafic lava composition. The Gamma Ray Spectrometer (GRS) onboard the *Mars Odyssey* spacecraft provides abundances for select elements (Boynton et al., 1992); however, the instrument has an effective field of view of ~500 km, and published maps are smoothed with a ~900 km boxcar filter (Boynton et al., 2007), so the signal from Aav is not isolated. Still, the published maps indicate that western Elysium Planitia, which includes Athabasca Valles and Cerberus Palus, is marked by low potassium and thorium concentrations and a relatively high iron abundance (Boynton et al., 2007), consistent with mafic lavas. An important caveat to these results is that they are the average composition of the upper ⩽0.5 m, of which a significant fraction may be surficial windblown deposits. In fact, the high-chlorine signature of these lava plains has been attributed to either this dust layer or the contamination of pixels by adjacent chlorine-rich MFF materials to the south (Diez et al., 2009).

In contrast to GRS data, the mineralogical maps produced by the Compact Reconnaissance Imaging Spectrometer for Mars (CRISM) instrument onboard *MRO* have ample spatial resolution to isolate the Aav signal. CRISM can operate in a number of different modes, including "multispectral survey", "half resolution", and "full resolution". In the full-resolution targeted (FRT) mode, the spatial resolution is usually 15–19 m/pixel and the spectral resolution is 6.55 nm/channel from 362 to 3920 nm (Murchie et al., 2007). The calibrated and map-projected CRISM data and browse maps of different mineral indices have been made available online by the CRISM Team.

All overlapping HiRISE and CRISM-FRT observations of Aav surfaces were carefully examined. The HiRISE data were used to identify low-dust areas in the CRISM images. Unfortunately, none of these images provides an unambiguous signal in the standard mineral indices developed (and made available via browse products) by the CRISM Team. The only automated detection is a weak signature for high-calcium pyroxene on talus slopes within the Cerberus Fossae at the head of Athabasca Valles (where both Aav and underlying strata contribute to the talus) in FRT0000851B (Fig. 4).

In an effort to extract additional constraints from the CRISM data, spectra of Aav were compared to the nearest *in situ* compositional measurements of lava – those made by the Mars

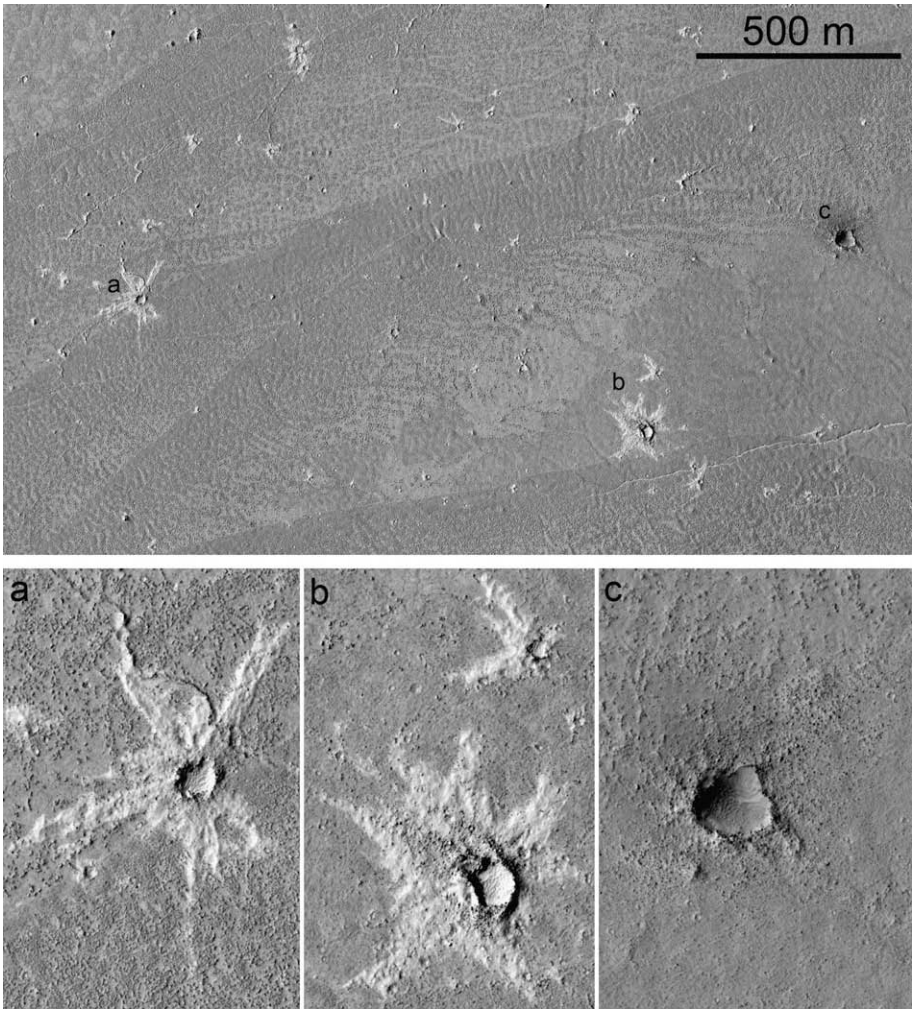

Fig. 2. Subsection of HiRISE image PSP_001408_1900. North is up; illumination is from the left. The scene is located immediately north of the easternmost fissure vent from which the Athabasca Valles flood lava (Aav) erupted. Thin, broad lobes of lava cover the region. They are speckled with small impact craters, many of which have rays of relatively bright material associated with their ejecta blankets. The bright ejecta is slightly elevated above the surrounding lava, and its asymmetry indicates oblique impacts from the east (a and b). This type of crater expression is fairly characteristic of Zunil secondaries across the region, and it likely indicates that the region was thinly mantled at the time of the impact event. In contrast, other populations of craters do not have elevated, bright material preserved in their ejecta blankets (c).

Exploration Rover (MER) *Spirit* in Gusev crater (Fig. 1). Although the floor of Gusev crater was initially hypothesized to comprise a lacustrine deposit, *Spirit* data revealed that it was instead covered by an extensive lava flow (Squyers et al., 2004). Utilizing visible, infrared, Mössbauer, and X-ray spectroscopy, McSween et al. (2004, 2008) characterized these "Adirondack" type lavas as having a composition intermediate to a basalt and a picrobasalt. Another spectrally relevant surface that *Spirit* studied was the "El Dorado" ripple field. The sand in the ripples is highly mafic and is relatively dust free (Sullivan et al., 2008), providing a cleaner example of what an olivine- and pyroxene-rich material looks like in CRISM data.

Two sites were selected where HiRISE images show the least dusty outcrops of Aav over areas large enough for CRISM to resolve. These locations exhibit a distinctly blue tone in the HiRISE enhanced color products, and it is noteworthy that this blue color has been broadly correlated with mafic rocks (Delamere et al., this issue). The first site is a crater 1.1 km in diameter that impacted into Aav, exposing rock and ejecting boulders. Both the slopes in the wall of the crater and those on many boulder faces are sufficiently steep to minimize dust accumulation. The second site is within the Cerberus Fossae (FRT000851B, mentioned above), where backwasting has produced an extensive talus slope composed of Aav, underlying strata, and wind-transported materials. Unfortunately, neither site provides a clean, aerially extensive outcrop of Aav.

For analysis, the released reduced-data records (in *I*/*F* units) for both the shorter and longer CRISM wavelengths were ingested into the Integrated Software for Imagers and Spectrometers, Version 3 (ISIS3) developed by the US Geological Survey (Anderson et al., 2004). The worst noise (vertical striping and signal drift) was removed using the *cubenorm* program. In lieu of a formal atmospheric correction, the spectrum of interest was divided (ratioed) by the spectrum of a nearby patch of bright dust. Average spectra from polygons of interest were then extracted using the interactive *qview* program. Thus, these spectra are not absolute reflectivity but rather brightness relative to the dusty background.

The spectral similarity between the least dusty parts of Aav and the highly mafic surfaces analyzed by *Spirit* are unmistakable (Fig. 5). Moreover, the broad absorption from the visible toward 1 μm is typical of mafic minerals, especially olivine (e.g., Clark et al., 1993). Nevertheless, this analysis is inadequate to identify specific minerals. It only shows that the CRISM data are consistent with the hypothesis that Aav is spectrally similar to the mafic–ultramafic materials seen by *Spirit* in Gusev crater.

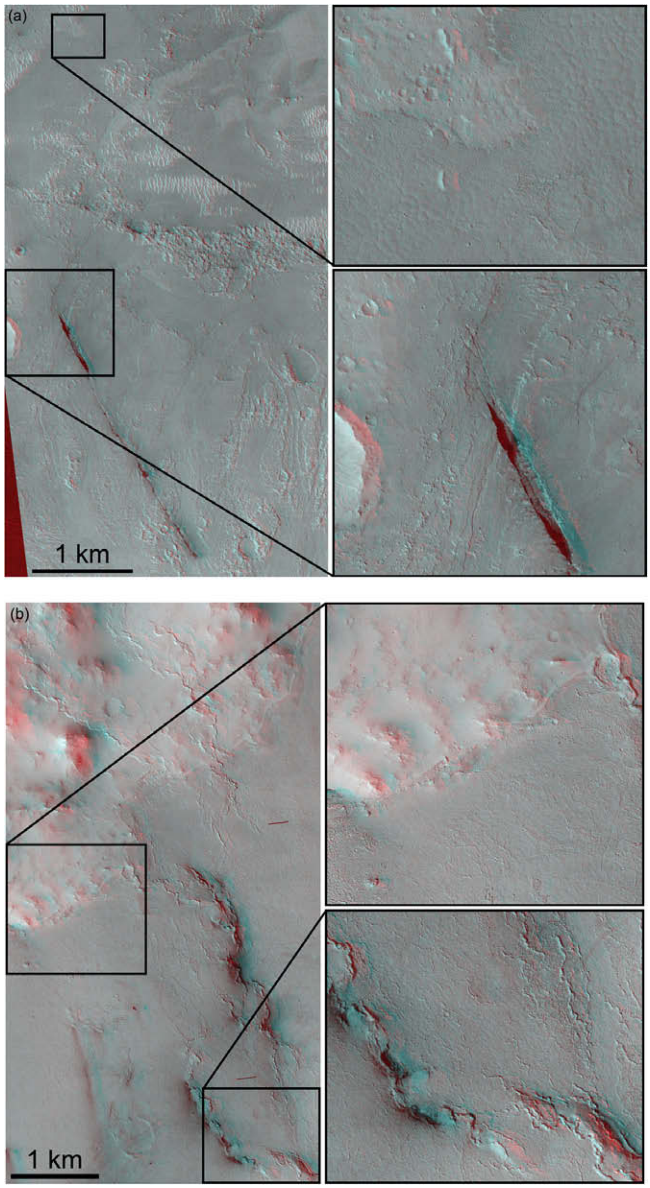

Fig. 3. (a) Subsection of an anaglyph produced from HiRISE stereo image pair PSP_003650_1900 and PSP_004283_1900. The scene is located near the head of Athabasca Valles. The Aav flood lava coats all but the western and northwestern edges of the anaglyph. In the southern half of the anaglyph, a pair of graben-bounding faults oriented SE–NW cuts the lava surface. The offset along the faults is relatively minor. The insets to the right show the flow margin of the Aav flood lava (top and bottom) and the deepest part of the graben (bottom) in more detail. (b) Subsection of an anaglyph produced from HiRISE stereo image pair PSP_003914_1890 and PSP_004191_1890. The scene is located at the northern edge of Cerberus Palus. A wrinkle ridge system runs roughly N–S through the anaglyph, crossing the contact between Aav and the rim of an older impact crater. Kinematic indicators in the lava signify that the ridges were present at the time Aav was emplaced. However, pronounced brittle deformation along parts of the ridge axes suggests that compressive deformation continued after the lava solidified. The insets at the right show the Aav flow margin, which stands higher than the deflated surface of the lava flow (top), and a portion of the ridge system that appears to have been active subsequent to Aav emplacement (bottom).

The mafic–ultramafic mineralogy tentatively suggested by the CRISM data is consistent with the low viscosities (10^0–10^5 Pa s) derived from modeling of adjacent plains volcanism (Vaucher et al., 2009). Although such model-derived viscosities can differ markedly from rigorous laboratory measurements, they are self-consistent and can be compared to viscosities calculated using the same techniques for terrestrial lavas of known composition (e.g., Hulme, 1974; Fink and Zimbelman, 1986). In this context, the viscosity estimates of Vaucher et al. (2009) indicate highly mafic lavas. Thus, separate analyses done on different lava flows within Elysium Planitia point to a mafic–ultramafic compositional range, suggesting some degree of regional continuity in lava type.

A final piece of evidence that is consistent with, though again not diagnostic of, a mafic–ultramafic composition for Aav comes from the Shergotty, Nakhla, and Chassigny (SNC) meteorites from Mars. These are all mafic–ultramafic igneous rocks, with several likely to be from young lava flows (e.g., Nyquist et al., 2001). Collectively, these samples of the martian surface are suggestive of the composition of typical lava flows on Mars; however, it is impossible to directly equate the SNC meteorites with Aav.

Given the lack of better alternatives, the Adirondack-type Gusev lavas are used as the preferred compositional analog for the Athabasca Valles flood lava in the flow modeling presented below in Section 3. However, a full range of mafic to ultramafic compositions is also examined for the sake of completeness.

2.3. Extent and volume of Aav

Before the acquisition of *MRO* data, the extent of Aav was difficult to determine because of the need for vast coverage at high spatial resolution. As noted above, the unit is very thin within proximal Athabasca Valles (Jaeger et al., 2007), and it increases to only a few tens of meters thick where it ponded in Cerberus Palus (Murray et al., 2005), perhaps reaching a maximum thickness of 50 m in the narrow arm of the flow that abuts Aeolis Planum (Lanz and Saric, 2009). Because the flow thickness tapers toward its margins, topographic data from the Mars Orbiter Laser Altimeter (MOLA) are unable to reliably identify the margin of the flow. Moreover, because the surrounding terrain consists mostly of young lava flows, Aav is not typically characterized by a distinct thermal inertia in Thermal Emission Imaging System (THEMIS; Christensen et al., 2004) infrared data. The margins of the flow are well resolved in Mars Orbiter Camera (MOC; Malin et al., 1992) and HiRISE images; however, these datasets provide insufficient coverage to map the full extent of the unit. THEMIS Visible images are locally useful, but the 18 m/pixel scale and relatively poor signal to noise ratio of many images limits their overall utility. Fortunately, the Context (CTX) imager onboard *MRO* has the requisite mix of high spatial resolution and wide area coverage (Malin et al., 2007). Contacts seen in the HiRISE and MOC images can be readily identified in the ~6 m/pixel CTX images and confidently extended across their typically ~30 km swath width and >100 km length.

More than 300 CTX images have been processed using ISIS3 and then imported into the ESRI ArcMap geographic information system (GIS) software package. With these data and tools, the margin of Aav has been traced essentially continuously from source to terminus. In areas where the contact is difficult to discern in CTX, supporting HiRISE and MOC observations were utilized. The only portion of the flow margin with significant gaps in coverage is along the northwestern edge of the flow, but fortunately this is an area where THEMIS data are generally adequate. The largest uncertainties in the location of the Aav flow margin are not due to coverage gaps, but rather a buried contact along its southern edge. A ~400-km-long discontinuous section of the contact is buried by MFF materials around the northern edge of Zephyria Planum. It is difficult to estimate precisely how much of Aav is buried, but it is unlikely to be a significant amount. The vast majority of the MFF is older than Aav (e.g., Tanaka et al., 2005), and consequently, Aav cannot extend beneath these older sections of MFF. This constraint limits the maximum extent of buried Aav to ~3000 km^2, which corresponds to a ~1% uncertainty.

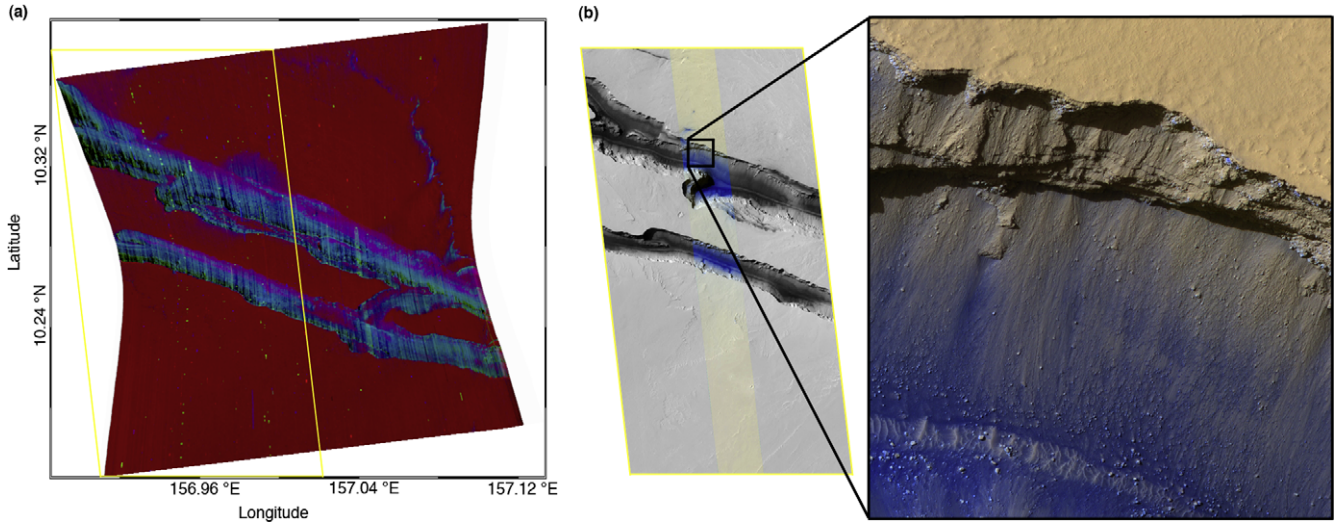

Fig. 4. (a) CRISM browse product showing mafic mineralogy for observation FRT0000851B. Red is the olivine mineral index, green is low-calcium pyroxene, and blue is high-calcium pyroxene. Most of the region is sufficiently dusty to preclude any characterization of its mineralogy. The reddish appearance of the dust-covered plains probably does not indicate that the dust is olivine rich. Rather, it is likely to be an artifact of the image stretch. However, the blue zones on the northern walls of the Cerberus Fossae do hint at the presence of high-Ca pyroxene in the sandy, rocky talus slopes. The green regions on the south walls of the fissures are confined to areas that are in shadow; they are unlikely to reflect the true composition of the surface. The yellow box shows the footprint of the HiRISE image displayed to the right. (b) Central portion of HiRISE image PSP_009557_1905. North is up; illumination is from the left. The high-Ca pyroxene signature seen in the CRISM observation corresponds to the bluish talus in the HiRISE enhanced color data. The inset on the far right shows the talus in greater detail; it is composed of scattered boulders and widespread sands that are bluer than their surroundings. (For interpretation of the references to color in this figure legend, the reader is referred to the web version of this article.)

With the exception of the aforementioned areas, the location of the flow margin is generally known to better than 100 m, often to ~10 m. The confidence with which the flow margin can be followed obviates the need to rely on indirect inferences such as subtle changes in crater densities or surface textures. However, Aav is consistently less cratered than many other young lavas in the area that issued from both small vents (the Cerberus Tholi) and other segments of the Cerberus Fossae.

Fig. 6 shows the mapped extent of Aav. The path the lava took is quite complex: it started from several locations (though just 2 major vents) along the Cerberus Fossae, flowed into Athabasca Valles, exploited breaches in the wrinkle ridge confining Athabasca Valles, surrounded Persbo crater, debouched into Cerberus Palus, exited through spillways to the south and east, and was then diverted around the complex pre-existing topography as the lava extended to both the southeast and west. One striking difference between Aav and well-mapped terrestrial flood lavas (e.g., the Roza Member of Wanapum Basalt, Self et al., 1997; Thordarson and Self, 1998) is that Aav does not appear to be a compound flow field composed of multiple distinct lava flows. Instead, it appears that Aav was emplaced during a single event, despite the many bifurcations and confluences in the lava flow. For example, even though the lava that flowed through Athabasca Valles was fed by multiple eruptive vents, no flow margin is visible, where the lavas from these different sources converged. This indicates that the fissure vents were simultaneously active.

The total surface area of Aav, as it is mapped, is 250,000 km^2, making it slightly larger than the combined area of the Great Lakes situated along the US–Canada border. In linear distance, the farthest extent of the lava from the source is ~1100 km, but lava was transported a minimum of 1400 km to reach this point. Volume estimates are less certain because flow thickness cannot be directly measured, however some indirect measurements have been made. The bulk of Aav resides in the Cerberus Palus basin at the foot of Athabasca Valles, making that the most crucial area to investigate. Based on the size of craters that were draped by (and therefore show through) the Aav flood lava, Murray et al. (2005) estimated a pre-deflation flow depth of ~45 m in Cerberus Palus and a current (post-deflation) flow depth of ~30 m. This is consistent with the present topography of Cerberus Palus, which includes a closed depression about 12 m deep with a volume of ~1000 km^3 (Lanagan, 2004). This may reflect the volume of material that drained out of Cerberus Palus as the flow extended to the west and southeast. If the entire Aav flood lava were 30 m thick, it would translate to a volume of 7500 km^3. However, this is an upper bound on the flow volume since the lava is substantially thinner within Athabasca Valles and along its margins. A more realistic average thickness of 20 m would suggest a volume of 5000 km^3, though marginally smaller volumes are plausible.

By comparison, the best mapped flood basalt flow on Earth, the Roza Member of the CRB Group, has a volume of 1300 km^3, an area of 40,300 km^2, and a maximum lava transport distance of ~300 km (Tolan et al., 1989; Thordarson and Self, 1998). The largest known flood lava flows on Earth connect the Deccan and Rajahmundry Traps on opposite sides of the Indian subcontinent and span a total distance of ~1000 km. While outcrops are limited, individual flow fields are estimated to have covered 80,000–185,000 km^2 and may have exceeded 5000 km^3 (Self et al., 2008). Thus, the Athabasca Valles flood lava appears to be more aerially extensive than the largest flood lavas on Earth but has a similar volume. Still, it covers less than a quarter of the >10^6 km^2 Elysium Planitia volcanic province (Plescia, 1993).

3. Emplacement of the Athabasca Valles flood lava

The near-perfect plan-view exposure of Aav, coupled with the good topographic coverage of Athabasca Valles, provides an unrivaled opportunity to study the style and dynamics of flood-lava emplacement. The general methodology we follow in our modeling is described in more detail in Keszthelyi et al. (2006), where the physical properties of the lava and the dimensions of the channel are used to estimate flow velocity and lava flux. From this, and

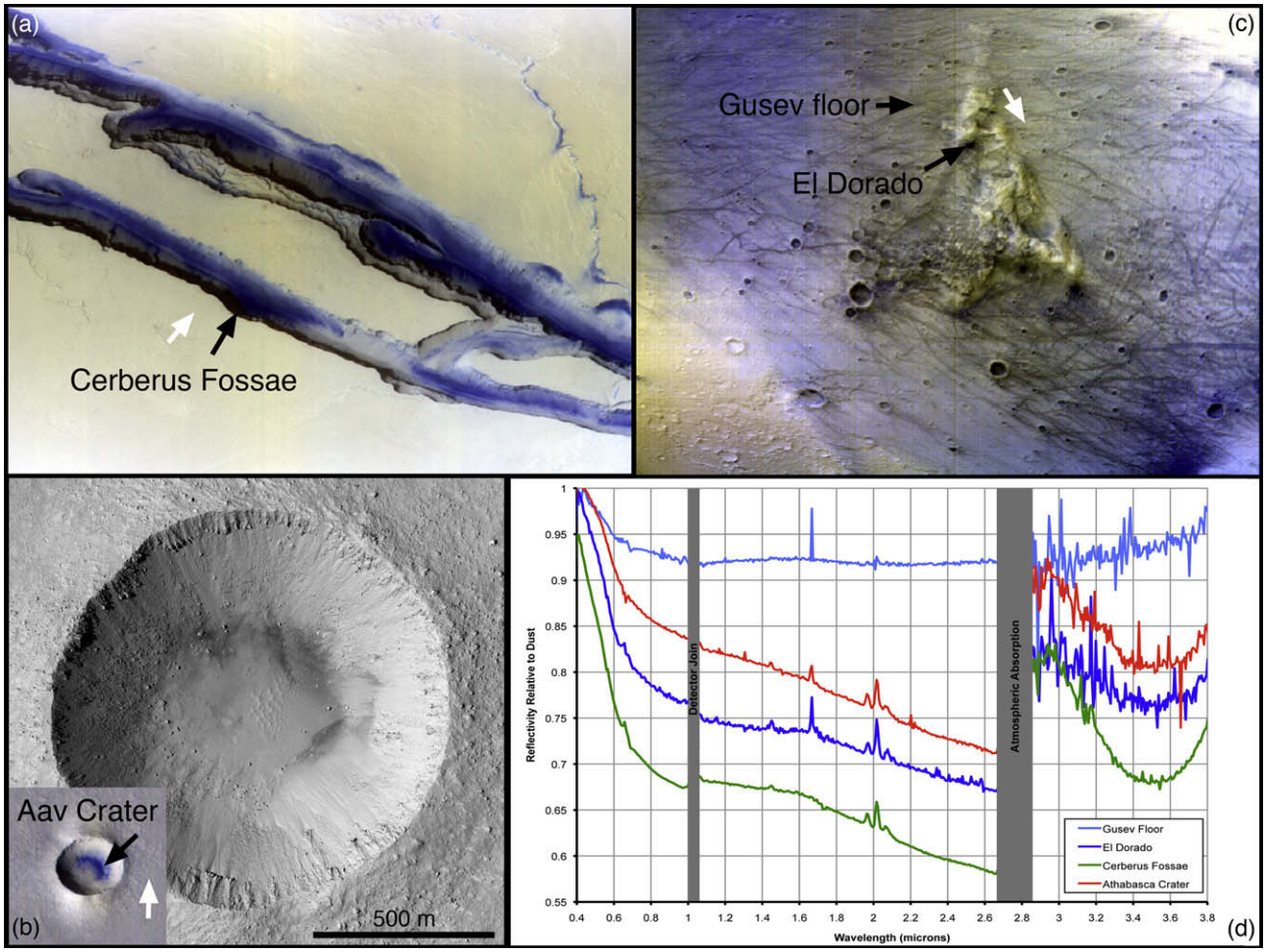

Fig. 5. Comparison of CRISM spectra from Aav and the MER *Spirit* landing site in Gusev crater. (a) CRISM FRT 0000851B over the Cerberus Fossae at the head of Athabasca Valles; the fractures walls are covered with a talus slope of lava boulders as well as eolian sands (cf. Fig. 4). The CRISM data are unprojected but have been rotated so north is approximately at the top of the image. Spatial resolution varies between ~22 and 18 m/pixel within each observation because the viewing geometry changes significantly during the acquisition of an FRT. Red, green, and blue channels are displaying bands 25 (~520 nm), 55 (~715 nm), and 95 (~980 nm), respectively. The black arrow points to the region from which a spectrum was extracted. The white arrow indicates the region from which the reference dusty spectrum was extracted. (b) Fresh ~1 km diameter impact crater on the Aav in the medial portion of Athabasca Valles as seen in HiRISE observation PSP_006907_1890 and CRISM FRT 000063D5. CRISM data is displayed in the same manner as (a). The background is from HiRISE image PSP_006907_1890. Note the mix of boulders and sand in the area from which the CRISM spectrum was extracted (arrow). (c) CRISM FRT 0000929F over the Columbia Hills and surrounding terrain in Gusev crater. Again the data are presented in the same manner as (a) and (b). One CRISM spectrum was obtained from the intersection of dust-devil tracks in order to minimize the amount of dust. The other spectrum comes from the El Dorado ripple field. (d) CRISM spectra (relative to the bright background) color-coded for each site. The smaller grey bar covers the join between the shorter (VNIR) and longer (IR) portions of the spectra where neither detector appears to provide reliable data. An empirical multiplicative adjustment was made to join the VNIR and IR spectra. The second wider grey bar covers an atmospheric absorption band that effectively blocks the signal from the ground. The negative slope in the VNIR portion of the spectrum is unusual for Mars (which is generally brighter in the redder part of the spectrum). This spectral slope, which produces a blue color in the HiRISE enhanced color products and the CRISM data as displayed in (a)–(c), is consistent with (but not diagnostic of) absorption bands from mafic minerals, especially olivine (e.g., Sullivan et al., 2008). This slope is less pronounced (at longer wavelengths) on the floor of Gusev crater because even at the intersection of two dust devil tracks the ground is covered with optically significant amounts of dust. (For interpretation of the references to color in this figure legend, the reader is referred to the web version of this article.)

the known volume of the flow, an eruption duration can be calculated. These results can then be cross-checked against various other observations.

3.1. Physical properties of the Aav lava

As discussed in Section 2.1, the lavas in Gusev crater are the closest source of *in situ* data from which to estimate the physical properties of the Aav flood lava. Greeley et al. (2005) tabulate the thermal and physical properties of the Adirondack-type Gusev lavas, of which viscosity and density are needed for flow modeling. The viscosity of the liquid lava, at the liquidus temperature of 1270 °C, was estimated to be 2.8 Pa s. With bubbles and cooling (and crystallization), Greeley et al. (2005) suggest that a value of 50 Pa s might be more realistic for the bulk viscosity of the lava during emplacement. By comparison, Hawaiian basalts usually have bulk viscosities of 10^2–10^4 Pa s, including the effect of a thin crust (e.g., Shaw et al., 1968; Heslop et al., 1989; Gregg and Keszthelyi, 2004). Viscosities of 10–100 Pa s are considered in the following modeling, with 50 Pa s being the preferred value. This large range of viscosities covers the uncertainties in lava composition.

It should be noted that the rheology of lava is often more complex than can be described by a single value such as Newtonian viscosity. Many studies have shown that lava can exhibit a yield strength, a strain-rate dependent viscosity, and viscoelastic properties. These complications are most evident when the lava has cooled and has a substantial solidified component. However, for the near-vent section of Aav, and given the inferred highly mafic composition, these effects are likely to be negligible compared to the order-of-magnitude range of viscosities already being considered.

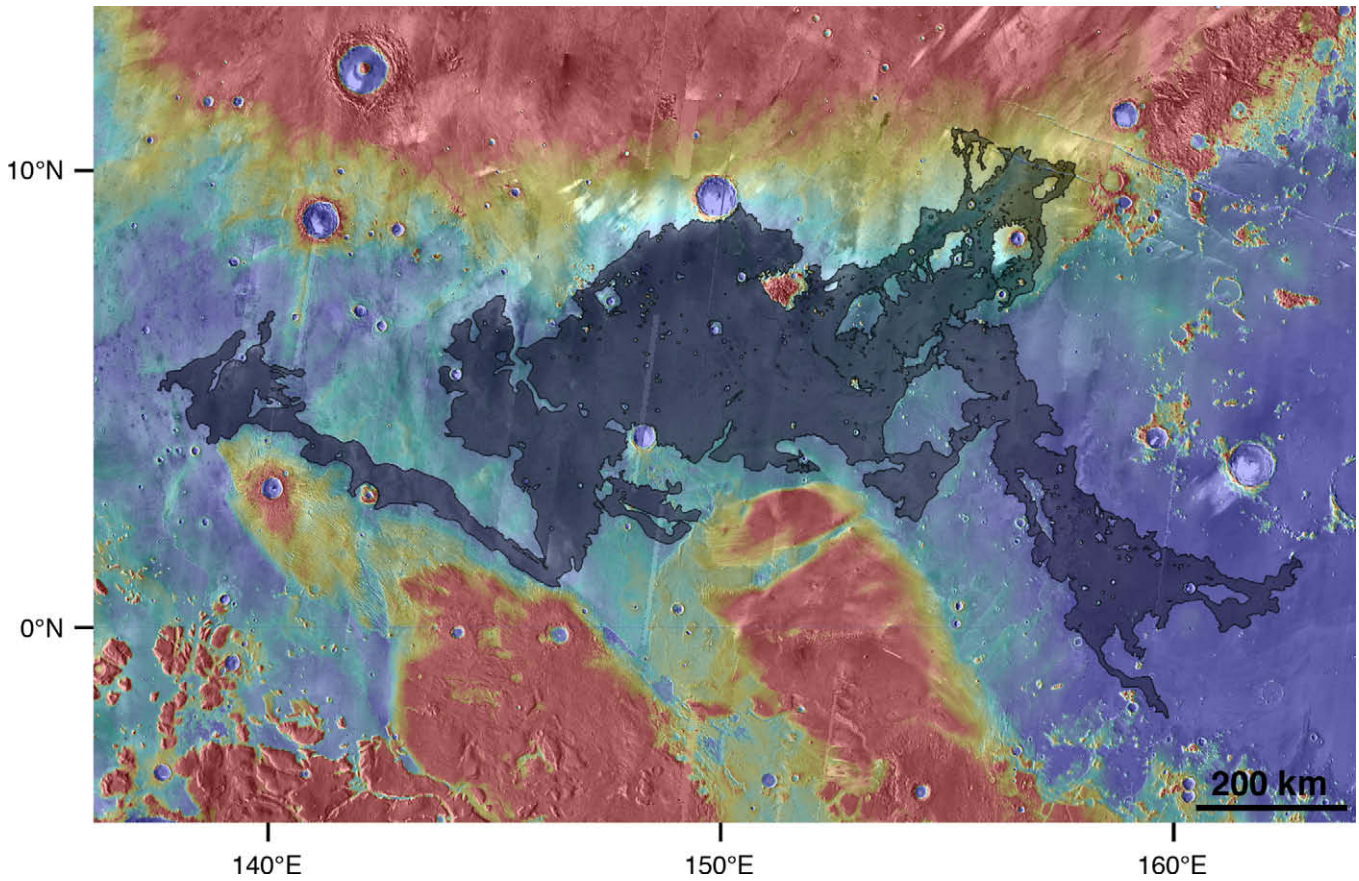

Fig. 6. Extent of the Aav flood lava, as mapped from MRO data. The basemap is a global 256 m/pixel THEMIS daytime IR mosaic colorized with MOLA gridded data. The margin of the Aav flood lava was traced in an ArcGIS project, relying on the >300 released CTX images in this region.

Greeley et al. (2005) calculate a liquid density of 2820 kg/m^3 for the Gusev lava at liquidus. Although partial crystallization during cooling can produce higher density minerals, the bulk density of flowing lava is most profoundly affected by bubble content. Typical mafic lava flows have 20–50 vol.% bubbles (e.g., Self et al., 1998; Keszthelyi et al., 2004). However, near the vent, bubble content can exceed 70 vol.% (e.g., Swanson, 1973; Mangan and Cashman, 1996). Bubble contents of 20–70 vol.% are considered in our modeling, yielding bulk densities of 2300–850 kg/m^3, with 1400 kg/m^3 as the preferred value.

3.2. Channel dimensions and high-lava stands

Following the approach taken by earlier studies of aqueous flood discharge through Athabasca Valles (e.g., Burr, 2003), hydraulic modeling is focused on the upper section of the channel system, before sizeable distributaries were established (Fig. 7). The vast majority of Aav lava must have passed through this segment of the channel, and geologic mapping suggests that the lava was running bank-full at peak discharge (i.e., high-lava marks are coincident with the top of the channel banks). MOLA profiles through this part of the channel show an average channel depth of ~45 m and channel widths of 30–50 km. The average slope through the region is well constrained by MOLA to be 0.063 ± 0.007%.

Although MOLA provides excellent information on ⩾10-km-scale topographic features, kilometer-scale data gaps exist in Athabasca Valles (Keszthelyi et al., 2007). This introduces uncertainties in determining the elevation of Aav flow margins (i.e., high-lava marks) seen in HiRISE and CTX images. In order to obtain higher quality topographic data, the US Geological Survey produced digital elevation maps (DEMs) of portions of the upper channel using stereo imagery from both CTX and HiRISE. The HiRISE DEM (Figs. 8 and 9) was constructed from stereo observations PSP_002661_1895 and PSP_003294_1895, using techniques described in Kirk et al. (2008). It has 1-m postings and a vertical precision of better than 0.5 m. The largest errors are related to the joins between CCDs in each observation, where steps of a few tens of centimeters can occur. The CTX DEM (Fig. 9) is the first of its kind and was collected at a spatial resolution of 20 m/post. The production methodology is similar to that for HiRISE DEMs (Kirk et al., 2008), but has not been fully documented at present. Overall, the quality of the CTX DEM is excellent, but some artifacts can be seen in deep shadows (where there is no information) and in the form of kilometer-wavelength ripples in the northern part of the DEM caused by undocumented motions of the spacecraft.

The HiRISE DEM allows flow depths in the main channel to be precisely measured. Within the coverage of this DEM, the maximum lava flow depth was 80 ± 1 m; however, a comparison of lava-capped topographic highs in the DEM with individual MOLA shots outside the DEM suggests that the lava locally reached 97 ± 10 m in depth (Fig 8). This reflects the variability in channel floor topography. An interesting observation is that the lowest point in this DEM is the center of an impact crater that has been filled by lava. Murray et al. (2005) noted a similar topographic expression in impact craters in Cerberus Palus and suggested that such volume loss could not be explained by a lava flow. We suggest that bubble loss after the emplacement, but prior to the solidification, of the lava may explain these observations. In such a scenario, the greatest volume loss would occur where the flow was thickest, in this case at the center of the crater.

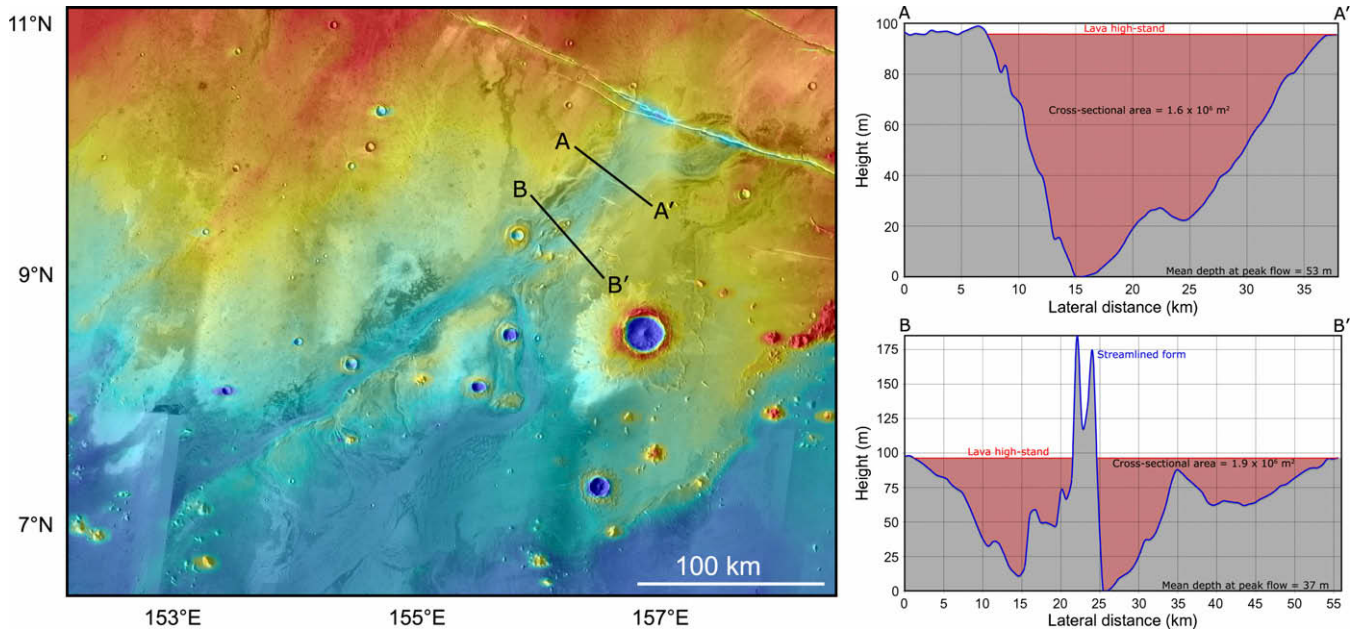

Fig. 7. Two of several MOLA profiles used to estimate the depth and cross-sectional area of proximal Athabasca Valles. In the graphs to the right, the substrate is represented in gray and the lava, shown at its highest stand, in red. Although some Aav lava circumvented this part of the channel system, those flows were confined to minor tributaries. An implicit assumption in the calculation of flow depth and cross-sectional area is that the present topography is similar to that at the time the Aav lava coursed through the channel (i.e., deflation left Aav very thin in this part of the channel, and the lava did not significantly erode the substrate). (For interpretation of the references to color in this figure legend, the reader is referred to the web version of this article.)

The CTX DEM is located downstream of the HiRISE DEM, where the largest distributary channel in Athabasca Valles breaches a wrinkle ridge to split from the main channel (Fig. 9a). An examination of high-lava marks around a prominent impact crater within the channel shows that the lava ran ~75 m higher on the upstream side than the downstream side (Fig. 9b). One possible explanation is that the large number of flow obstacles in this part of the channel caused the lava to back-up. This was suggested to have occurred during the aqueous flood that is hypothesized to have carved Athabasca Valles (Burr, 2003). Alternatively, the lava level may have been elevated due to the confluence of a smaller flow with the main channel immediately north of the impact crater. Either way, this "superelevation" of the flow surface provides important clues to the local flow dynamics that are beyond the scope of the current study.

3.3. Flow regime and velocity

The equations for flow through a channel are fundamentally different for laminar and turbulent flow. For laminar flow of a Newtonian fluid, the average flow velocity through a wide channel is given by

$$\langle v\rangle = \rho g \sin(\theta) H^2/3\eta \quad (1)$$

where $\langle v\rangle$ is the mean flow velocity, ρ is the bulk density, g is gravitational acceleration, θ is slope, H is flow depth, and η is viscosity (e.g., Bird et al., 1960). For turbulent flow, the average flow velocity is characterized by the deceptively simple equation

$$\langle v\rangle = [gH\sin(\theta)/C_f]^{1/2} \quad (2)$$

where C_f is the friction factor (e.g., Goncharov, 1964). Note that the average turbulent flow velocity is not explicitly dependent on density or viscosity and is much less sensitive to changes in flow thickness, slope, and gravity than laminar flow is.

The difficulty in calculating the average turbulent flow velocity lies in determining the friction factor. Typically, C_f values are of order of 0.001–1.0 for a variety of natural and engineering cases (Baloga et al., 1995 and references therein). Values between 0.0057 and 0.11 were calculated for some rapidly emplaced Hawaiian flows (Baloga et al., 1995), but it is not clear that these flows were actually turbulent. An alternative method of deriving C_f that is applicable to moderately turbulent flow was obtained empirically by Goncharov (1964). In this method, C_f is expressed as a function of the Reynolds Number (Re)

$$C_f = (1/32)\left(\log_{10}(6.15(2Re+800)/41)^{0.92}\right)^{-2} \quad (3a)$$

$$Re = \rho H\langle v\rangle/\eta \quad (3b)$$

This expression is valid for channel flow for $500 < Re < 10{,}000$ though it may be extended with some caution to higher values. The transition from laminar to turbulent flow begins at a Re of 500–2000 for most channel or pipe flows with natural roughness. However, fully turbulent flow, where inertial forces fully dominate viscous forces, may not be achieved until a Re of 10^4 or more, especially for flow over very smooth surfaces (e.g., Bird et al., 1960). Because the flow is only moderately turbulent in the Goncharov (1964) laboratory experiments, viscosity and flow density, as parts of the Reynolds Number, do play a weak role in governing flow velocity. This is the formulation used by Shaw and Swanson (1970) to investigate the turbulent emplacement of the Roza flow in the CRB. Note that, since C_f is dependent on $\langle v\rangle$, Eqs. (2) and (3) must be solved recursively.

Fig. 10 shows the calculated flow velocity through the upper part of Athabasca Valles at maximum discharge using Eqs. (1) and (2). Table 1 shows how some of the key flow parameters vary with choice of input value. These calculations indicate that, at peak discharge, the flow was marginally to fully turbulent (Re = 860–300,000) over the full range of the input values for the physical properties of the lava. For reasonable choices, the friction factor is predicted to be about 0.003–0.01, producing average flow velocities around 5–10 m/s.

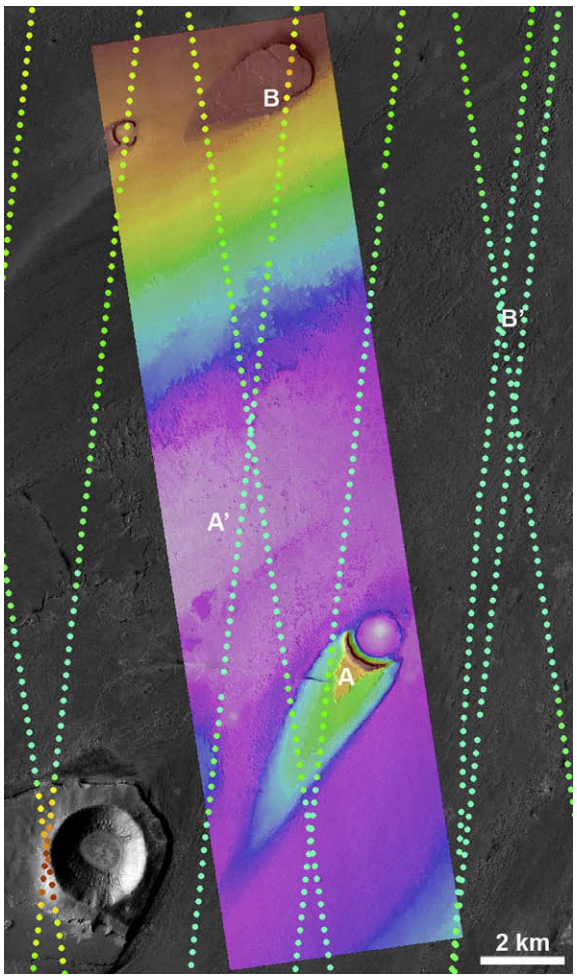

Fig. 8. HiRISE stereo DEM and MOLA shots in proximal Athabasca Valles. The DEM (with colorized topography) was produced from observations PSP_002661_1895 and PSP_003294_1895 at 1 m posting. The colorized topography is overlain on an orthorectified version of PSP_003294_1895, which in turn is overlain on CTX image P01_001606_1997. MOLA shot points are placed over the image data (the circle diameters are roughly the size of MOLA footprints). The light purple area in line with A′–B′ highlights deepest part of the channel. The maximum flow depth within the DEM is 80 m, measured between A (−2525 m) and A′ (−2605 m). However, the margin of Aav is at −2491 ± 10 m at location B, and B′ is at an elevation of −2588 m, indicating that the lava was locally ~100 m deep. Over the short span between A′ and B′, the slope is 0.2%, much steeper than the average for the entire channel (~0.063%). The elevations are presented in a non-linear color stretch to qualitatively accentuate topographic features.

3.4. Peak eruption rate and eruption duration

Because proximal Athabasca Valles has an average cross-sectional area of 1–2 × 10^6 m^2 between the high-lava marks on opposite banks (Fig. 7), the estimated flux of lava through the channel is 5–20 × 10^6 m^3/s. Since turbulent flow is quite insensitive to the properties of the fluid, it is not surprising that these results are similar to the 1–2 × 10^6 m^3/s estimated for the discharge of an aqueous flood through this section of Athabasca Valles (Burr, 2003; Keszthelyi et al., 2007). At the 5–20 × 10^6 m^3/s rate, it would have taken 3–17 days to erupt the entire 5000–7500 km^3 of the Aav flood lava. For most terrestrial fissure eruptions, the average eruption rate is nearly an order of magnitude less than the peak discharge (e.g., Wadge, 1981; Thordarson and Self, 1993), suggesting that an eruption duration of 1–6 months might be more likely. In any case, the estimated duration is significantly shorter than the ~10 years suggested by Keszthelyi et al. (2000, 2004) or, similarly, the decade timescale of some terrestrial flood lava eruptions (e.g., Self et al., 1997; Thordarson and Self, 1998), but similar to older estimates for continental flood lavas that involved turbulent flow (Shaw and Swanson, 1970).

3.5. Supporting evidence for a short eruption duration

The conclusion that a flood-lava flow was emplaced as a short-lived, turbulent flood is sufficiently heretical to require corroborating evidence. Several qualitative observations do support this result. The most basic is the fact that Aav is a "simple flow," as opposed to a "compound flow field" composed of multiple lobes (Walker, 1971). The deflation of the flow, leaving only a thin lava drapery in proximal Athabasca Valles, is also consistent with a short flow duration. As noted earlier, the observation that lava from separate sources along the Cerberus Fossae merges together (rather than crosscuts) indicates that the eruption took place as a single event, rather than as a series of distinct episodes in an extended eruption. Another common characteristic of longer duration flows is extensive inflation (Hon et al., 1994; Self et al., 1998). Evidence for inflation within Aav is confined to its most distal reaches (i.e., locations where the flow may have been fed by the draining of Cerberus Palus for some time after the eruption at the vent had ended).

A quantitative piece of supporting evidence comes from a slab of tilted crust seen in HiRISE stereo pair: PSP_001540_1890 and PSP_002371_1890 (Fig. 11). The slab was upended when a hydrovolcanic (rootless) cone was built on the thin crust of the Aav flood lava, causing it to crack and founder under the load. The absence of wakes on the downstream side of the cone indicates that it is a late-stage feature; that is, it formed after the crust had ceased rafting (Jaeger et al., 2007). Using shadow measurements and the known positions of the spacecraft and the Sun, basic trigonometry shows that this slab was tilted to about a 40–45° angle. The apparent thickness of the slab is just a few pixels in the 29 cm/pixel HiRISE images. Correcting for foreshortening, the actual thickness is estimated to be 50–150 cm. These values are consistent for both HiRISE images.

The numerical lava-cooling model of Keszthelyi and Denlinger (1996) was used to estimate the time required to form a lava crust of the observed thickness. The model uses a fully explicit finite-difference algorithm, it includes crystallization and glass formation as well as temperature- and bubble-dependent thermal properties, and it accounts for cooling by thermal radiation and wind. The only parameters changed from the field-verified terrestrial cases were ambient temperature (set to −50 °C), lava temperature (1250 °C), glass transition temperature (1050 °C), and the atmospheric heat transfer coefficient (1 $W m^{-2} K^{-1}$). The model output indicates that it would take ~3–24 days to form a crust 50–150 cm thick (Fig. 12). An important caveat to this result is that a stable crust could only have started to grow once the lava flow was quiescent enough not to autobrecciate it, so the output timescale is a hard lower limit to, not an estimate of, the eruption duration. However, this result does provide strong evidence that the waning phase of the eruption, which is typically the longest part, was quite short for Aav. In conclusion, there is strong evidence for (and no evidence contraindicating) a short eruption duration. In fact, the supporting evidence suggests that the eruption duration was on the short end of the estimated range, with the most likely duration being a few to several weeks.

4. Conclusions

The Athabasca Valles flood lava is the only well-documented case of a turbulently emplaced flood-lava flow. With this example in hand, other examples of turbulent lavas can be sought on Earth

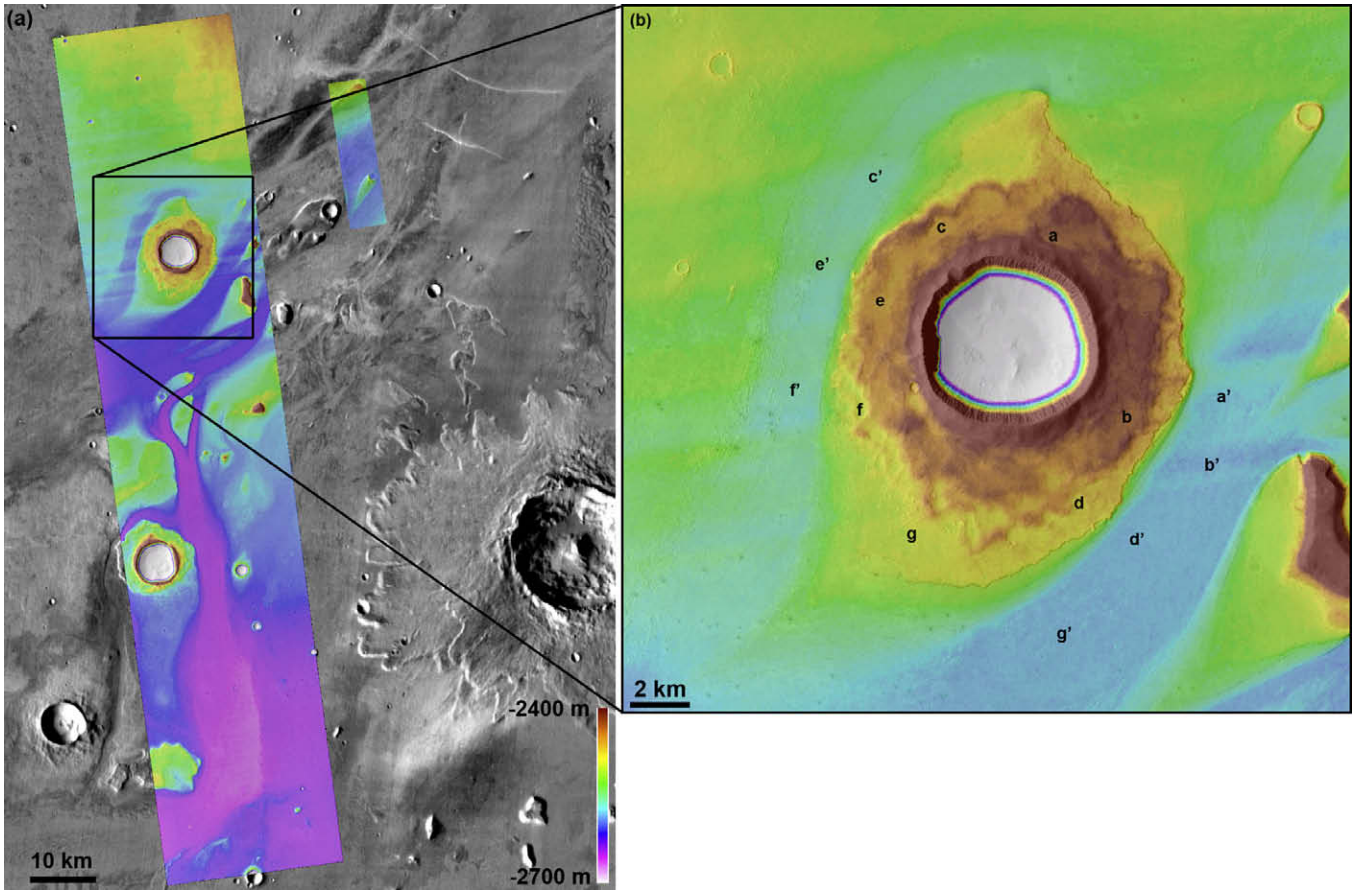

Fig. 9. (a) HiRISE and CTX DEMs overlain on a mosaic of 100 m/pixel THEMIS daytime IR data. Elevations are presented in a consistent linear color scheme for both DEMs. (b) Close-up of an impact crater whose ejecta blanket was eroded into a streamlined shape when Athabasca Valles was carved. The flow divided around the crater, with the northern branch having a floor ~30 m above the southern one (−2585 m vs. −2615 m). The gradient in both channels is too small to measure. In contrast with the near-horizontal floor, the high-lava marks on the ejecta blanket vary by ~75 m from the upstream end (a = −2457 m) to the downstream point (g = −2533 m). Flow depth at b–b′ was nearly 150 m, dropping to ~105 m by d–d′ and ~80 m by g–g′. By comparison, the flow depth holds at 100 ± 10 m along c′–f′. The elevations are presented in a non-linear color stretch to qualitatively accentuate topographic features.

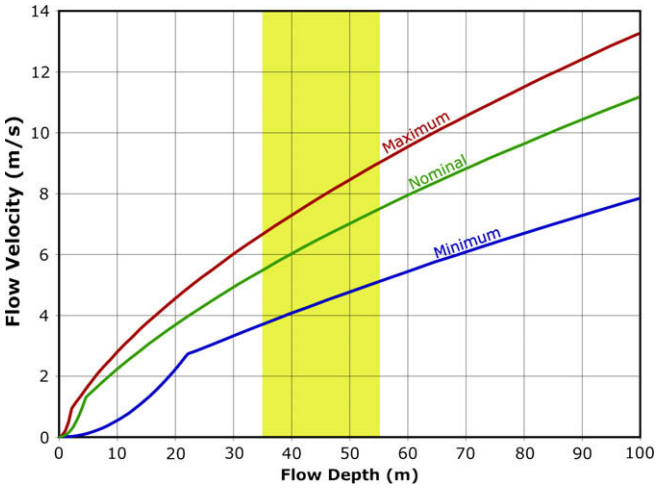

Fig. 10. Graph illustrating lava flow velocity as a function of flow depth at peak discharge for proximal Athabasca Valles. The green trend shows the nominal results, and the red and blue lines encompass the uncertainties. The kinks in the trends demarcate the transition from laminar to turbulent flow. The yellow swath covers the mean channel depth range of 45 ± 10 m. This range corresponds to a mean velocity for the Aav lava at peak discharge of ~4–9 m/s, with a nominal value of 7 m/s. At the center of the channel where the flow was deepest, the lava may have been traveling upwards of 10 m/s. (For interpretation of the references to color in this figure legend, the reader is referred to the web version of this article.)

Table 1
Variation in lava flow velocity, Reynolds Number (Re), and the friction factor (C_f) as a function of flow depth, viscosity, density and channel slope. The wide range of input values produces a relatively narrow range of flow velocities, all of which are consistent with turbulent flow.

Flow depth (m)	Viscosity (Pa s)	Density (kg/m^3)	Slope (%)	Velocity (m/s)	Re	C_f
30	10	2300	0.070	5.9	41,000	0.0044
30	50	1400	0.063	4.2	3600	0.0078
30	100	850	0.056	3.4	860	0.0110
45	10	2300	0.070	7.8	81,000	0.0038
45	50	2300	0.063	6.1	13,000	0.0075
45	50	1400	0.070	6.0	7600	0.0064
45	50	1400	0.063	5.7	7100	0.0066
45	50	1400	0.056	5.3	6700	0.0066
45	50	850	0.063	5.3	4000	0.0075
45	100	850	0.056	4.5	1700	0.0094
60	10	2300	0.070	9.5	130,000	0.0035
60	50	1400	0.063	6.9	12,000	0.0058
60	100	850	0.056	5.5	2800	0.0083
100	10	2300	0.070	13.0	300,000	0.0030
100	50	1400	0.063	9.9	28,000	0.0048
100	100	850	0.056	7.9	6700	0.0067

and Mars. One of the key characteristics that may help identify other such flows is the great distance (>200 km) to which the deflated lava facies extends away from the vent. Similar features are seen around basaltic eruptions at Kilauea Volcano, Hawaii,

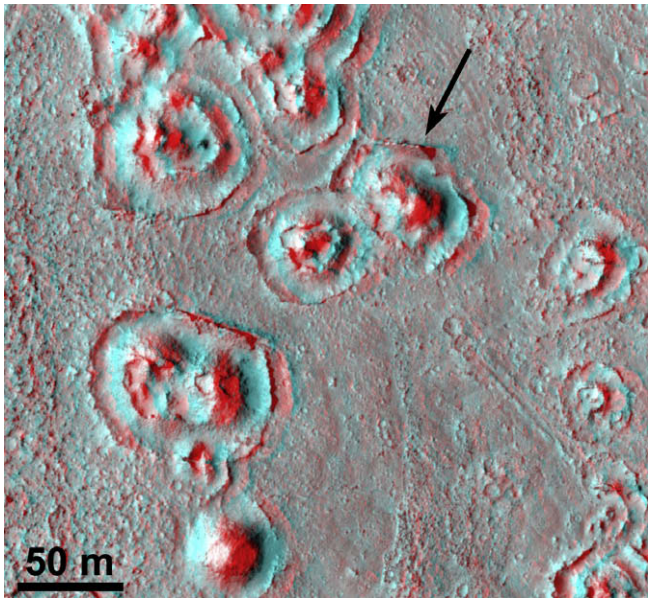

Fig. 11. Sub-region of an anaglyph produced from HiRISE stereo image pair PSP_001540_1890 and PSP_002371_1890. The arrow points to a thin plate that appears to be oriented nearly vertically, though in reality it is only tilted ~40–45°. The plate is a piece of the solidified crust of the Aav flood lava that was broken and upended in response to the loading of the lava surface by the growth of a hydrovolcanic (rootless) cone.

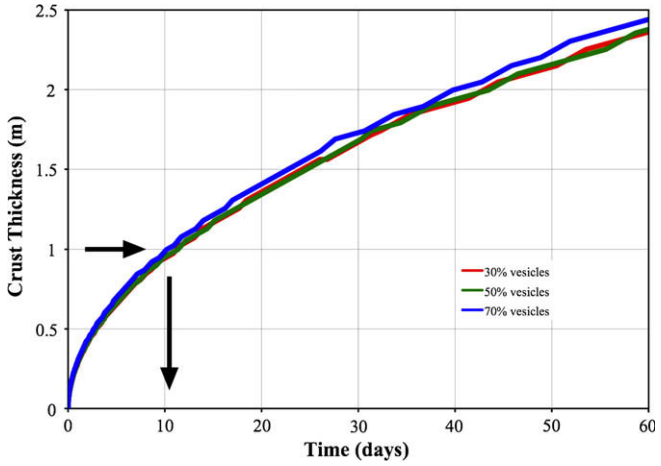

Fig. 12. Graph showing lava crust growth as a function of time. Output is from the Keszthelyi and Denlinger (1996) numerical cooling model adjusted for martian conditions as described in the text. Colored curves show the small effect of varying vesicularity, which is the model parameter that has the greatest effect on cooling rate. Over timescales of days, the reduced atmospheric cooling more than compensates for the lower ambient temperature, leading to a lava cooling marginally slower on Mars than on Earth. The black arrows show that the ~1 m thick tilted slab seen in Fig. 10 would take ~11 days to form. (For interpretation of the references to color in this figure legend, the reader is referred to the web version of this article.)

but they only extend a few hundred meters from the vent (e.g., Swanson, 1973; Heslop et al., 1989). Although it is a very distinctive feature, this large section of deflated lava may be difficult to identify in less pristine cases because the thin lava carapace can be relatively easily eroded, covered, or otherwise obscured.

An eruption duration of only a few to several weeks raises the question of how this volume of lava can be brought to the surface in such a short time. Clearly, the magmatic plumbing system must have been unusual in some way. The length of fissure that appears to have been simultaneously active was ~160 km, giving a peak eruption rate per unit length of dike of 30–120 m^2/s. For comparison, the rate for the 1783–1784 Laki eruption in Iceland and the Roza Member of the CRB Group are estimated to have been ~1–2 m^2/s during the vigorous phases (e.g., Thordarson and Self, 1993; Self et al., 1997). This suggests an unusually large dike by terrestrial standards, but well within theoretical limits. Wilson and Head (2002) investigated the dikes hypothesized to underlie the major graben systems on Mars (such as the Cerberus Fossae). They found that individual dikes could be 50–500 m wide, contain 2–6 $\times 10^4$ km^3 of magma, and be fed at rates approaching 10^9 m^3/s. Thus, the dike capacity seems more than adequate, and the challenge becomes supplying magma to such a dike from the source region. The key may be the presence of voluminous magma chambers, presumably at great depth, but further study is required.

Continued examination of the martian surface with HiRISE shows that Grjotá, Rahway, and Marte Valles (Fig. 1) are all also draped by platy-ridged flood lavas. Similar but significantly more degraded lava fill is seen within Ma'adim Vallis and Gusev crater just south of Elysium Planitia and in Mangala Valles south of Amazonis Planitia. Lava can also be seen within Kasei Valles to the east of the Tharsis volcanoes. Thus, Athabasca Valles is only the most pristine example of a process that seems to have taken place in many channel systems on Mars.

One key point that HiRISE has not yet resolved is the role of erosion by lava in the large channel systems. This work shows that the eruption rates involved in the emplacement of turbulent flood lavas are similar to the discharge rates estimated for the aqueous floods that are generally thought to have performed the channel incision. This certainly opens the possibility, as suggested by Leverington (2004), that erosion by lava could have been significant. The short duration of the Aav eruption argues against thermal erosion, but mechanical erosion by lava may be effective (Ciesla and Keszthelyi, 2000; Siewert and Ferlito, 2008). The erosive potential of an aqueous flood is typically proportional to the total stream power (Ω), given by the formula

$$\Omega = \rho g Q \alpha \tag{4}$$

where ρ is the fluid density, g is gravitational acceleration, Q is the volumetric flux through the channel, and α is the slope (e.g., Baker and Costa, 1987). Since the estimated flux of lava is similar to or even greater than that estimated for the aqueous floods through Athabasca Valles, and since lava has a density similar to or higher than water, the total stream power of the lava should have been similar to or greater than that estimated for aqueous floods. Thus, it would seem very likely that, at peak discharge, Aav was able to efficiently transport any loose particles. However, the erosion of bedrock involves fundamentally different processes, including plucking and cavitation (e.g., Baker, 2009). Features indicative of bedrock erosion, such as cataracts, are seen in Athabasca Valles (Keszthelyi et al., 2007). At this point, it is not known if cavitation can occur in a relatively viscous three-phase fluid like lava at the estimated values for *Re*, nor have the dynamics of turbulent eddies in lava been investigated. Until further studies are completed, the idea of lava flow erosion remains merely an intriguing possibility.

Acknowledgments

We are grateful to all those who have been involved in building and operating the *MRO* spacecraft, and particularly its HiRISE instrument. We also thank the numerous people at the US Geological Survey's Astrogeology Program who have worked on ISIS programming and DEM production. Financial support for this work was provided by the MRO project, the Mars Data Analysis program and the Planetary Geology and Geophysics program.

References

Anderson, J.A., Sides, S.C., Soltesz, D.L., Sucharski, T.L., Becker, K.J., 2004. Modernization of the integrated software for imagers and spectrometers. Lunar. Planet. Sci. Conf. XXXV (Abstract #2039).

Baker, V.R., 1973. Paleohydrology and Sedimentology of Lake Missoula Flooding in Eastern Washington. Geol. Soc. Am. Spec. Pap. 144, 79 pp.

Baker, V.R., 2009. The channeled scabland: A retrospective. Ann. Rev. Earth Planet. Sci. 37, 6.1–6.19.

Baker, V.R., Costa, J.E., 1987. Flood power. In: Mayer, L., Nach, D. (Eds.), Catastrophic Flooding. Allen and Unwin, London, pp. 1–24.

Baloga, S., Spudis, P.D., Guest, J.E., 1995. The dynamics of rapidly emplaced terrestrial lava flows and implications for planetary volcanism. J. Geophys. Res. 100, 24509–24519.

Berman, D.C., Hartmann, W.K., 2002. Recent fluvial, volcanic, and tectonic activity on the Cerberus Plains of Mars. Icarus 159, 1–17.

Bird, R.B., Stewart, W.E., Lightfoot, E.N., 1960. Transport Phenomena. Wiley, New York.

Boynton, W.V., and 19 colleagues, 1992. Science applications of the Mars Observer Gamma Ray Spectrometer. J. Geophys. Res. 97, 7681–7698.

Boynton, W.V., and 27 colleagues, 2007. Concentrations of H, Si, Cl, K, Fe, and Th in the low- and mid-latitude regions of Mars. J. Geophys. Res. 112. doi:10.1029/2007JE002887.

Burr, D.M., 2003. Hydraulic modeling of Athabasca Vallis, Mars. Hydrol. Sci. J. 48, 655–664.

Basaltic Volcanism Study Project, 1981. Basaltic Volcanism on the Terrestrial Planets. Pergamon Press, Inc., New York.

Christensen, P.R., and 10 colleagues, 2004. The Thermal Emission Imaging System (THEMIS) for the Mars 2001 odyssey mission. Space Sci. Rev. 110, 85–130.

Ciesla, F.J., Keszthelyi, L., 2000. A simple model for lava flow quarrying: Mechanical erosion of the substrate. Lunar. Planet. Sci. Conf. XXXI (Abstract #1647).

Clark, R.N., Swayze, G.A., Gallagher, A.J., King, T.V.V., Calvin, W.M., 1993. The US Geological Survey Digital Spectral Library: Version 1: 0.3 to 3.0 microns. US Geol. Surv. Open File Rep. 93-592, 1340 pp. <http://speclab.cr.usgs.gov>.

Delamere, W.A., and 16 colleagues, 2009. Color imaging of Mars by the High Resolution Imaging Science Experiment (HiRISE). Icarus 205, 38–52.

Diez, B., Feldman, W.C., Mangold, N., Baratoux, D., Maurice, S., Gasnault, O., d'Uston, L., Costard, F., 2009. Contribution of Mars Odyssey GRS at Central Elysium Planitia. Icarus 200, 19–29.

Fink, J.H., Zimbelman, J.R., 1986. Rheology of the 1983 Royal Gardens basalt flows, Kilauea Volcano, Hawaii. Bull. Volcanol. 48, 87–96.

Geikie, A., 1880. The lava-fields of North-western Europe. Nature 23, 3–5.

Goncharov, V.N., 1964. Dynamics of Channel Flow. Translated from Russian by Israel Program Science Translation. US Department of Commerce, Office of Technical Services, Washington, DC.

Greeley, R., Foing, B.H., McSween, H.Y., Neukum, G., Pinet, P., van Kan, M., Werner, S.C., Williams, D.A., Zegers, T.E., 2005. Fluid lava flows in Gusev crater, Mars. J. Geophys. Res. 110. doi:10.1029/2005JE02401.

Gregg, T.K.P., Keszthelyi, L.P., 2004. The emplacement of pahoehoe toes: Field observations and comparison to laboratory simulations. Bull. Volcanol. 66, 381–391.

Hartmann, W.K., Neukum, G., 2001. Cratering chronology and the evolution of Mars. Space Sci. Rev. 96, 165–194.

Head III, J.W., Coffin, M.F., 1997. Large igneous provinces: A planetary perspective. In: Mahoney, J.J., Coffin, M.F. (Eds.), Large Igneous Provinces: Continental, Oceanic, and Planetary Flood Volcanism. American Geophysical Union, Washington, DC, pp. 411–438.

Heslop, S.E., Wilson, L., Pinkerton, H., Head, J.W., 1989. Dynamics of a confined lava flow on Kilauea Volcano, Hawaii. Bull. Volcanol. 51, 415–432.

Hon, K., Kauahikaua, J., Denlinger, R., Mackay, K., 1994. Observations and measurements of active lava flows on Kilauea Volcano, Hawaii. Geol. Soc. Am. Bull. 106, 351–370.

Hooper, P.R., 1982. The Columbia River basalts. Science 215, 1463–1468.

Hulme, G., 1973. Turbulent lava flows and the formation of lunar sinuous rilles. Modern Geol. 4, 107–117.

Hulme, G., 1974. The interpretation of lava flow morphology. Geophys. J. R. Astron. Soc. 39, 361–383.

Huppert, H.E., Sparks, R.S.J., 1985. Komatiites I: Eruption and flow. J. Petrol. 26, 694–725.

Jaeger, W.L., Keszthelyi, L.P., McEwen, A.S., Dundas, C.M., Russel, P.S., 2007. HiRISE observations of Athabasca Valles, Mars: A lava-draped channel system. Science 317, 1709–1711.

Jaeger, W.L., Keszthelyi, L.P., McEwen, A.S., Titus, T.N., Dundas, C.M., Russell, P.S., 2008. Response to Comment on "Athabasca Valles, Mars: A lava-draped channel system". Science 320, 1588.

Keszthelyi, L., Denlinger, R., 1996. The initial cooling of pahoehoe lava flows. Bull. Volcanol. 58, 5–18.

Keszthelyi, L., McEwen, A.S., Thordarson, Th., 2000. Terrestrial analogs and thermal models for martian flood lavas. J. Geophys. Res. 105, 15027–15050.

Keszthelyi, L., Thordarson, Th., McEwen, A., Haack, H., Guilbaud, M.-N., Self, S., Rossi, M., 2004. Icelandic analogs to martian flood lavas. Geochem. Geophys. Geosyst. 5. doi:10.1029/2004GC000758.

Keszthelyi, L., Self, S., Thordarson, Th., 2006. Flood lavas on Earth, Io, and Mars. J. Geol. Soc. London 163, 253–264.

Keszthelyi, L.P., Denlinger, R.P., O'Connell, D.R.H., Burr, D.M., 2007. Initial insights from 2.5D hydraulic modeling of floods in Athabasca Valles, Mars. Geophys. Res. Lett. 34. doi:10.1029/2007GL031776.

Kirk, R.L., and 18 colleagues, 2008. Ultrahigh resolution topographic mapping of Mars with MRO HiRISE stereo images: Meter-scale slopes of candidate Phoenix landing sites. J. Geophys. Res. 113. doi:10.1029/2007JE003000.

Komatsu, G., Kargel, J.S., Baker, V.R., 1992. Canali-type channels on Venus: Some genetic constraints. Geophys. Res. Lett. 19, 1415–1418.

Kreslavsky, M., 2008. Young populations of small craters on Mars: A case study. European Planetary Science Conference Abstracts, vol. 3, EPSC2008-A-00237.

Lanagan, P.D., 2004. Geologic History of the Cerberus Plains. Ph.D. Dissertation, University of Arizona, Tucson, 142 pp.

Lanz, J.K., Saric, M.B., 2009. Cone fields in SW Elysium Planitia: Hydrothermal venting on Mars? J. Geophys. Res. 114. doi:10.1029/2008JE003209.

Leverington, D.W., 2004. Volcanic rilles, streamlined islands, and the origin of outflow channels on Mars. J. Geophys. Res. 109. doi:10.1029/2004JE002311.

Malin, M.C., Danielson, G.E., Ingersoll, A.P., Masursky, H., Veverka, J., Ravine, M.A., Soulanille, T.A., 1992. Mars observer camera. J. Geophys. Res. 97, 7699–7718.

Malin, M.C., and 13 colleagues, 2007. Context camera investigation on board the Mars Reconnaissance Orbiter. J. Geophys. Res. 112. doi:10.1029/2006JE002808.

Mangan, M.T., Cashman, K.V., 1996. The structure of basaltic scoria and reticulite and inferences for vesiculation, foam formation, and fragmentation in lava fountains. J. Volcanol. Geotherm. Res. 73, 1–18.

McEwen, A.S., Preblich, B.S., Turtle, E.P., Artemieva, N.A., Golombek, M.P., Hurst, M., Kirk, R.L., Burr, D.M., Christensen, P.R., 2005. The rayed crater Zunil and interpretations of small impact craters on Mars. Icarus 176, 351–381.

McEwen, A.S., and 69 colleagues, 2009. The High Resolution Imaging Science Experiment (HiRISE) during MRO's primary science phase (PSP). Icarus 205, 2–37.

McSween, H.Y., and 34 colleagues, 2004. Basaltic rocks analyzed by the Spirit rover in Gusev crater. Science 305, 842–845.

McSween, H.Y., and 14 colleagues, 2008. Mineralogy of volcanic rocks in Gusev crater, Mars: Reconciling Mössbauer, Alpha Particle X-Ray Spectrometer, and Miniature Thermal Emission Spectrometer spectra. J. Geophys. Res. 113. doi:10.1029/2007JE002970.

Murchie, S., and 49 colleagues, 2007. Compact Reconnaissance Imaging Spectrometer for Mars (CRISM) on Mars Reconnaissance Orbiter (MRO). J. Geophys. Res. 112. doi:10.1029/2006JE002682.

Murray, J.B., and 11 colleagues, and the HRSC Co-Investigator Team, 2005. Evidence from the Mars Express High Resolution Stereo Camera for a frozen sea close to Mars' equator. Nature 434, 352–256.

Nyquist, L.E., Bogard, D.D., Shih, C.Y., Greshake, A., Stöffler, D., Eugster, O., 2001. Ages and geologic histories of martian meteorites. Space Sci. Rev. 96, 105–164.

Plescia, J.B., 1990. Recent flood lavas in the Elysium region of Mars. Icarus 88, 465–490.

Plescia, J.B., 1993. An assessment of volatile release from recent volcanism in Elysium, Mars. Icarus 104, 20–32.

Reidel, S.P., Fecht, K.R., 1987. The Huntzinger flow: Evidence of surface mixing of the Columbia River basalt and its petrogenetic implications. Geol. Soc. Am. Bull. 98, 664–677.

Reidel, S.P., Tolan, T.L., 1992. Eruption and emplacement of flood basalt: An example from the large-volume Teepee Butte Member, Columbia River Basalt Group. Geol. Soc. Am. Bull. 104, 1650–1671.

Richthofen, F., 1868. The Natural System of Volcanic Rocks. Towne and Bacon Printers, San Francisco.

Self, S., Thordarson, Th., Keszthelyi, L., Walker, G.P.L., Hon, K., Murphy, M.T., Long, P., Finnemore, S., 1996. A new model for the emplacement of Columbia River basalts as large inflated pahoehoe flow fields. Geophys. Res. Lett. 23, 2689–2692.

Self, S., Thordarson, Th., Keszthelyi, L., 1997. Emplacement of continental flood basalt lava flows. In: Mahoney, J.J., Coffin, M.F. (Eds.), Large Igneous Provinces: Continental, Oceanic, and Planetary Flood Volcanism. American Geophysical Union, Washington, DC, pp. 381–410.

Self, S., Keszthelyi, L., Thordarson, Th., 1998. The importance of pahoehoe. Ann. Rev. Earth Planet. Sci. 26, 81–110.

Self, S., Jay, A.E., Widdowson, M., Keszthelyi, L.P., 2008. Correlation of the Deccan and Rajahmundry Trap lavas: Are these the longest and largest lava flows on Earth? J. Volcanol. Geotherm. Res. 172, 3–19.

Shaw, H.R., Swanson, D.A., 1970. Eruption and flow rates of flood basalt. In: Gilmore, E.H., Stradling, D.F. (Eds.), Proceedings of the Second Columbia River Basalt Symposium. East. Wash. State Coll. Press, Cheney, pp. 271–299.

Shaw, H.R., Wright, T.L., Peck, D.L., Okamura, R., 1968. The viscosity of basaltic magma: An analysis of field measurements in Makaopuhi lava lake, Hawaii. Am. J. Sci. 226, 225–264.

Siewert, J., Ferlito, C., 2008. Mechanical erosion by flowing lava. Contemporary Phys. 49, 43–54.

Squyers, S.W., and 49 colleagues, 2004. The Spirit rover's Athena science investigation at Gusev crater, Mars. Science 305, 794–799.

Sullivan, R., and 10 colleagues, 2008. Wind-driven particle mobility on Mars: Insights from Mars Exploration Rover observations at "El Dorado" and surroundings at Gusev crater. J. Geophys. Res. 113. doi:10.1029/2008JE003101.

Swanson, D.A., 1973. Pahoehoe flows from the 1969–1971 Mauna Ulu eruption, Kilauea Volcano, Hawaii. Geol. Soc. Am. Bull. 84, 615–626.

Tanaka, K.L., Skinner Jr., J.A., Hare, T.M., 2005. Geologic map of the northern plains of Mars. USGS Scientific Investigations Map (SIM) 2888, scale 1:15,000,000.

Thordarson, Th., Self, S., 1993. The Laki (Skaftár Fires) and Grímsvötn eruptions in 1783–1785. Bull. Volcanol. 55, 233–263.

Thordarson, Th., Self, S., 1998. The Roza Member, Columbia River Basalt Group: A gigantic pahoehoe lava flow field formed by endogenous processes? J. Geophys. Res. 103, 27411–27445.

Tolan, T.L., Reidel, S.P., Beeson, M.H., Anderson, J.L., Fecht, K.R., Swanson, D., 1989. Revisions to the estimates of the areal extent and volume of the Columbia River Flood Basalt Province. In: Reidel, S.P., Hooper, P.R. (Eds.), Volcanism and Tectonism in the Columbia River Flood-Basalt Province. Geological Society of America, Boulder, pp. 1–20 (Spec. Pap. 239).

Tyrrell, G.W., 1937. Flood basalts and fissure eruption. Bull. Volcanol. 1, 87–111.

Vaucher, J., Baratoux, D., Toplis, M.J., Pinet, P., Mangold, N., Kurita, K., 2009. The morphologies of volcanic landforms at Central Elysium Planitia: Evidence for recent and fluid lavas on Mars. Icarus 200, 39–51.

Wadge, G., 1981. The variation of magma discharge during basaltic eruptions. J. Volcanol. Geotherm. Res. 11, 139–168.

Walker, G.P.L., 1971. Compound and simple lava flows and flood basalts. Bull. Volcanol. 35, 579–590.

Washington, H.S., 1922. Deccan traps and the other plateau basalts. Geol. Soc. Am. Bull. 33, 765–804.

Wilson, L., Head, J.W., 2002. Tharsis-radial graben systems as the surface manifestation of plume-related dike intrusion complexes: Models and implications. J. Geophys. Res. 107. doi:10.1029/2001JE001593.

Wilson, L., Head, J.W., 2008. Volcanism on Mercury: A new model for the history of magma ascent and eruption. Geophys. Res. Lett. 35. doi:10.1029/2008GL035620.